Showcasing a study on a sulfide electrode material for lithium-ion batteries by a group of researchers led by Prof. Fang Lian from University of Science and Technology Beijing and Dr Xingjiang Liu from Tianjin Institute of Power Sources, P. R. China.

Sulfide cluster vacancies inducing an electrochemical reversibility improvement of titanium disulfide electrode material

TiS_2 with a sulfide cluster-vacancy (CV-TiS_{2-x}) has been calculated and prepared to explore a novel strategy to improve the electrochemistry reversibility of a sulfide electrode. Its stable crystal structure with broadened interlayer space ensured by the cluster vacancy, as well as the enhanced anionic redox reaction activity facilitates the lithium intercalation and deintercalation in the host structure, resulting in the significantly improved capacity and prolonged cycle life.

As featured in:

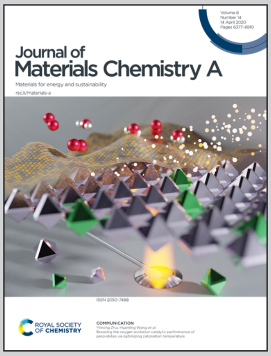
Journal of Materials Chemistry A

See Fang Lian, Xingjiang Liu *et al.*, *J. Mater. Chem. A*, 2020, **8**, 6532.

ROYAL SOCIETY OF **CHEMISTRY**

rsc.li/materials-a

Journal of
Materials Chemistry A

PAPER

Cite this: *J. Mater. Chem. A*, 2020, **8**, 6532

Sulfide cluster vacancies inducing an electrochemical reversibility improvement of titanium disulfide electrode material†

Jianhao Lu,[a] Fang Lian,*[a] Yuxuan Zhang,[a] Ning Chen,[a] Yang Li,[b] Fei Ding[b] and Xingjiang Liu*[b]

Received 18th November 2019
Accepted 17th January 2020

DOI: 10.1039/c9ta12631g

rsc.li/materials-a

Promoting the reversible structural transformation and carrier migration dynamics simultaneously in a multiple ion-involved process is vital for sulfide electrode materials. Herein, TiS_2 with a sulfide cluster vacancy (CV–TiS_{2-x}) has been calculated and prepared to explore a novel strategy to improve the electrochemistry reversibility of sulfide electrodes. It is found that the cluster vacancy can serve as an effective control factor for the improvement of the Fermi level, and enhances the electrochemical stability of CV–TiS_{2-x} in the liquid organic electrolyte system. Moreover, owing to the plentiful positively charged S-vacancies, the CV–TiS_{2-x} samples exhibit an extended interplanar spacing and retain their structural integrity during the lithium ion insertion process. The integrated HRTEM, *in situ* XRD, XPS analysis and electrochemical study reveal that the cluster vacancy is not only responsible for an increase in reversible performance, but also boosting the anionic redox reaction of $(S_2)^{2-}$ species. Therefore, the CV–TiS_{2-x} electrode delivers a reversible capacity of 650 mA h g^{-1} for 300 cycles at a current density of 1C (220 mA g^{-1}). Our study provides a novel strategy of introducing sulfur cluster vacancies to improve the electrochemical activity of TiS_2, which can be applied to other sulfide electrodes.

Introduction

Titanium disulfide (TiS_2) was first proposed as an electrode material by Whittingham for lithium batteries due to its advantages of intercalation chemistry (about 220 mA h g^{-1} specific capacity).[1–3] In the initial study, Li/TiS_2 cells suffered from safety concern issues and fast capacity decay, which was caused by lithium dendrites and the structural deterioration of the electrode during electrochemical processes.[4–6] The introduction of $LiCoO_2$ by Goodenough and commercial applications by Sony in the 1990s boosted the development of lithium-ion batteries.[7,8] Nonetheless, the revival of interest in the original lithium metal anode has inspired researchers to re-examine the TiS_2 electrode.

The crystal structure of TiS_2 is attacked by the strong interaction between the intercalated Li$^+$ and sulfur anions in the host. More seriously, the ordered phase is inclined to break up into amorphous domains as more lithium ions insert into the layered TiS_2 due to strong lattice strain and huge volume expansion.[9,10] Moreover, recent research studies have revealed that ester-based solvents in the electrolytes will react with polysulfides, which accelerates the structural deterioration of TiS_2.[11,12] Therefore, TiS_2 as an electrode material is facing a great challenge to possess beyond a one-electron lithium storage reaction and simultaneously maintain structural stability and high reversibility.

Vacancy engineering may convert electrodes with poor electrochemical activities into functionally active electrodes. In general, vacancy defects are almost inevitable during the solid state synthesis process of oxide or sulfide materials, especially in non-stoichiometry.[13] Single vacancies prefer to coalesce into clusters lowering the energy of the system.[14,15] The presence of a cluster vacancy not only helps to decrease the coordination number of the neighboring sites, but also affects the electronic structure of the material.[16–18] In a previous report, a cluster vacancy is responsible for converting a MoS_2 electrode into one with zinc storage capacity.[19] So far, there are only limited literature reports on the fundamental comprehension of cluster vacancies in sulfide electrode materials.

In this work, the effects of a sulfide cluster vacancy on the local structural evolution and lithium storage mechanism of TiS_2 have been investigated. We introduce a facile solid-state method to prepare TiS_2 microparticles with abundant sulfur vacancies (CV–TiS_{2-x}). DFT calculations and integrated characterization from HRTEM and *in situ* XRD are combined for a better understanding of the vacancy-induced electrochemical behavior. The results demonstrate that the CV–TiS_{2-x} sample

---

[a] *School of Materials Science and Engineering, University of Science & Technology Beijing, Beijing 100083, PR China. E-mail: lianfang@mater.ustb.edu.cn*

[b] *Science and Technology on Power Sources Laboratory, Tianjin Institute of Power Sources, Tianjin 300384, PR China*

† Electronic supplementary information (ESI) available. See DOI: 10.1039/c9ta12631g

with a sulfur cluster vacancy obtains a more positive Fermi energy level, leading to its electrochemical stability in an ether-based electrolyte. The electrochemical kinetics process has also been explored by EIS and GITT analysis, indicating the remarkably improved Li-ion diffusion coefficient (10^{-7} cm^2 s^{-1}) in CV–TiS$_{2-x}$. Furthermore, the vacancies promote the participation of the sulfur atoms in the redox reaction during cycling, with the anionic contribution of $[S–S]^{2-} \leftrightarrow 2S^{2-}$ transformation. Therefore, at the current of 1C (220 mA g^{-1}), a high reversible specific capacity (650 mA h g^{-1}) can be obtained in 300 cycles, which demonstrates the excellent reversible reaction of CV–TiS$_{2-x}$ during the charging and discharging processes. This work leads to a better understanding of vacancy engineering and opens up a way to develop transition metal sulfide electrodes towards long cycle life and high energy density.

Experimental

Calculations

In this work, density functional theory (DFT) calculations are carried out using Materials Studio with ultrasoft pseudopotentials and the generalized gradient approximation (GGA) exchange correlation functional parameterized by Perdew–Burke–Ernzerhof (PBE). A self-consistency convergence criterion of 10^{-5} eV is used for all calculations. All of the structures are fully relaxed until the force components on all atoms are less than 0.03 eV Å^{-1}. The number of plane waves is determined by a kinetic energy cut-off of 310 eV. Monkhorst–Pack grids with parameters of 2 × 2 × 1 are used to sample the Brillouin zone.

Material synthesis

The cluster vacancy TiS$_{2-x}$ (CV–TiS$_{2-x}$) is synthesized *via* a solid state reaction method under vacuum. Ti and S powders as precursors are ground together in a 1 : 1.95 atom ratio and the reaction formula can be summarized as follows:

$$\mathrm{Ti + S} \xrightarrow[550\ ^\circ\mathrm{C},1\mathrm{h}]{} \mathrm{TiS_2 + TiS_3} \xrightarrow[650\ ^\circ\mathrm{C},12\mathrm{h}]{} \mathrm{CV - TiS}_{2-x}$$

When heated, sulfur leaches out from the reactants through a sublimation process. The relationship between sulfur vacancy concentration and partial pressure of sulfur is shown in Fig. S1.† The reaction phase diagram during the preparation process is also shown in Fig. S2.† Finally, the obtained powder is washed with carbon disulfide (CS$_2$) first and then with absolute ethanol, centrifuged, and finally vacuum-annealed at 60 °C to obtain CV–TiS$_{2-x}$. TiS$_2$ purchased from Sigma-Aldrich with an ignorable amount of sulfur vacancies is employed as a vacancy-free sample (C–TiS$_2$) for comparison. Inductively coupled plasma-optical emission spectroscopy (ICP-OES) is used to determine the stoichiometry of C–TiS$_2$ and CV–TiS$_{2-x}$, and the molar ratio of Ti : S is calculated and presented in Table S1.†

Characterization and electrochemical measurements

The synthesized CV–TiS$_{2-x}$ and C–TiS$_2$ are analyzed by X-ray diffraction (XRD) using Cu Kα radiation (Bruker D2 Phaser diffractometer). The X-ray photoelectron spectroscopy (XPS) spectrum is tested on a Phoibos X-ray photoelectron spectrometer (100 Analyser, SPECS, Germany, Al Kα X-rays). The morphologies of TiS$_{2-x}$ are observed by field-emission scanning electron microscopy (FESEM) (JEOL 7500) and transmission electron microscopy (TEM) (JEOL 2010). Raman measurements are performed with a Raman JY HR800 Spectrometer.

The coin cells were assembled in an Ar-filled glovebox with a metallic–Li anode, a liquid electrolyte of LiTFSI (1 mol L^{-1}) in diethylene glycol dimethyl ether (DEGDME), and a cathode of 80% CV–TiS$_{2-x}$ or C–TiS$_2$ with 10% carbon and 10% polyvinylidene fluoride (PVDF) binder, and the tap density is 2.45 mg cm^{-2}. They are tested with a Land battery testing system at 25 °C, from 1.0 to 3.0 V. Electrochemical impedance spectroscopy (EIS), the galvanostatic intermittent titration technique (GITT) and cyclic voltammetry (CV) were carried out on an electrochemical workstation (VersaSTAT3).

Results and discussion

Fermi energy position, a major parameter in electronic structure, is studied using density of states (DOS) calculations to find the derivations induced by sulfur vacancies.[20–22] Fig. 1a–c show the DOS and projected density of states (PDOS) of vacancy-free, single vacancy and cluster vacancy TiS$_2$, respectively, obtained from calculation at the GGA level with PBE parametrization. Compared to the vacancy-free material, the single-vacancy sample shows a shift of the Fermi level toward the conduction band, which results from high electron accumulation.[23] However, the cluster vacancy sample exhibits an opposite shift of the Fermi level, which could be partially attributed to the overlap of the sulfur 3p states with the Ti 3d states (Fig. 1c). Additionally, the cluster vacancy sample exhibits strong hybridizations between the Ti 3d and S 3p states, which is induced by a significantly increased bonding strength between the neighboring S atoms and Ti atoms closest to the cluster.[24] The results demonstrate that the cluster vacancy induces changes in the electronic-state distribution, acting as an effective recombination center.

As shown in Fig. 1d, the determined Fermi levels are −1.23, −1.73, and −1.05 eV for the vacancy-free, single vacancy, and cluster vacancy samples, respectively. The more positive Fermi level makes the cluster vacancy TiS$_2$ a high chemical stability electrode for batteries. What's more, a large amount of sulfur vacancies is believed to make the TiS$_2$ host positively charged, which favors the rapid transport of Li$^+$ in the electrode and the stability of lithium–TiS$_2$ interaction.[25]

The CV–TiS$_{2-x}$ sample with cluster sulfur vacancies is synthesized by a facile solid-state reaction method. Thermogravimetric analysis (TGA) was carried out to determine the thermal stability of C–TiS$_2$ and CV–TiS$_{2-x}$ in an argon protection environment with a varying temperature range from 25 to 750 °C. As shown in Fig. S3,† a narrow dip occurs near 170 °C, which can be attributed to the removal of absorbed water. Then, a gentle and continuous weight loss can be observed from 350 to 750 °C, which is due to the devolatilization process. A minor weight loss of around 10% observed at 750 °C indicates the

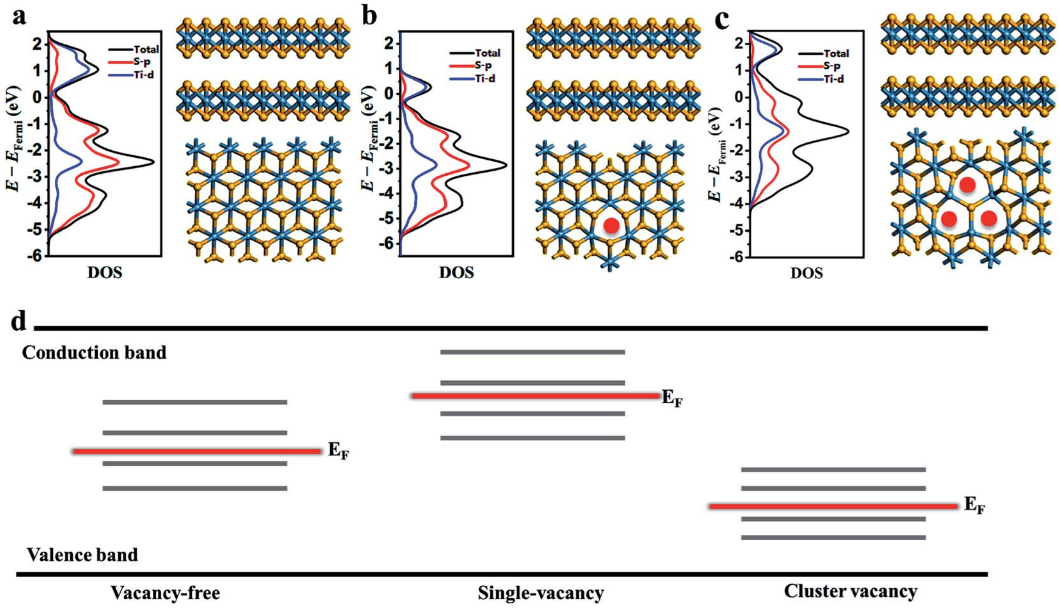

Fig. 1 DOS and PDOS on the sulfur p-orbitals and titanium d-orbitals of TiS_2: vacancy-free (a), single vacancy (b) and cluster vacancy (c). Scheme of the Fermi-level shift depending on the vacancy state (d).

good thermal stability of both samples. In addition, the lower value in weight loss of CV–TiS_{2-x} suggests that more sulfur vacancies exist in CV–TiS_{2-x} than C–TiS_2.[26] The crystal structures of CV–TiS_{2-x} and C–TiS_2 were investigated by Rietveld refined XRD as shown in Fig. 2a and S4,† respectively. The Bragg positions correspond well with the $P\bar{3}m1$ (No. 164) space group. The refinement results in Table S2† show that CV–TiS_{2-x} possesses a smaller cell volume, lower sulfur occupancy and shorter bond length than C–TiS_2, which is consistent with theoretical CV–TiS_{2-x} with a high concentration of sulfur vacancies. Furthermore, *ex situ* electron paramagnetic resonance (EPR) is employed to characterize the spin states of C–TiS_2 and CV–TiS_{2-x} in Fig. 2b. Unlike C–TiS_2, CV–TiS_{2-x} shows high intensity of the EPR peak at $g = 2.003$, which corresponds to its increased exposed active centers originating from the sulfide cluster vacancies.[27,28] Meanwhile, Raman spectroscopy, an effective route to characterize the defects, was employed to study CV–TiS_{2-x} and C–TiS_2. C–TiS_2 is demonstrated to have two Raman active modes consisting of an in-plane vibrational mode (E_g) and an out-of-plane mode (A_{1g}). In contrast, CV–TiS_{2-x} reveals three primary peaks, one at 226 cm^{-1} (assigned to E_g), one at 330 cm^{-1} (assigned to A_{1g}), and a "shoulder peak" at 372 cm^{-1} (Fig. 2c).[29] This suggests that the phonon modes are stiffened due to the appearance of abundant sulfur vacancies in TiS_2.[30]

The chemical binding environments of CV–TiS_{2-x} and C–TiS_2 were further evaluated by means of XPS analyses. These samples are etched to 30 nm in the direction from the surface toward the particle center in XPS measurement, and no binding energy peaks associated with $[S–S]^{2-}$ are detected in both samples. As shown in Fig. 2d, two strong peaks at 455.9 and 462.0 eV are observed for both CV–TiS_{2-x} and C–TiS_2. These two peaks are assigned to Ti $2p_{3/2}$ and Ti $2p_{1/2}$, respectively, matching closely the characteristic Ti^{4+} peaks. Another obvious pair of peaks for CV–TiS_{2-x} located at 463.2 and 458.1 eV corresponds to the reduction states of Ti^{3+} $2p_{1/2}$ and Ti^{3+} $2p_{3/2}$, respectively.[31] Fig. S5† presents three couples of fitted peaks located at 162.3, 161.1 and 160.6 eV, assigned to sulfur vacancies, S $2p_{3/2}$ and S $2p_{1/2}$ for CV–TiS_{2-x}.[32]

SEM, TEM and high resolution transmission electron microscopy (HRTEM) were employed to characterize the structure of CV–TiS_{2-x} as shown in Fig. S6† and 2e, respectively. The intensity profile along the red line in Fig. 2e shows sudden decreases of the continuous sulfur peaks in comparison with C–TiS_2 (Fig. 2f), demonstrating the existence of cluster vacancies in CV–TiS_{2-x}.

In situ XRD measurements were performed to monitor the structure evolution of CV–TiS_{2-x} and C–TiS_2, accompanying initial (Fig. S7†) and second cycling (Fig. 3a), respectively. According to the lithium ion occupation during cycling, a continuous change is observed in the stacking distance of the TiS_2 layers. The XRD patterns for the first cycle indicate that both electrodes undergo a solid solution process between the two phases of TiS_2 and $LiTiS_2$, which is consistent with previous work.[17,33] However, in the second cycle, the C–TiS_2 gradually exhibits an intermediate peak located at the angle of 22°, which is related to the nonconductive sulfur products. Since the electron accumulation decreases the Fermi level of C–TiS_2 to more negative potentials, the electron transfer may prefer the solvent molecule to the TiS_2 host,[34] which subsequently triggers a parasitic decomposition reaction of the electrolyte and damages the layer structure of C–TiS_2. In contrast, CV–TiS_{2-x} shows a stable structure during lithium deintercalation in DEGDME-based electrolyte. The cluster vacancy induces a much more positive shift of the Fermi level closer to the conduction

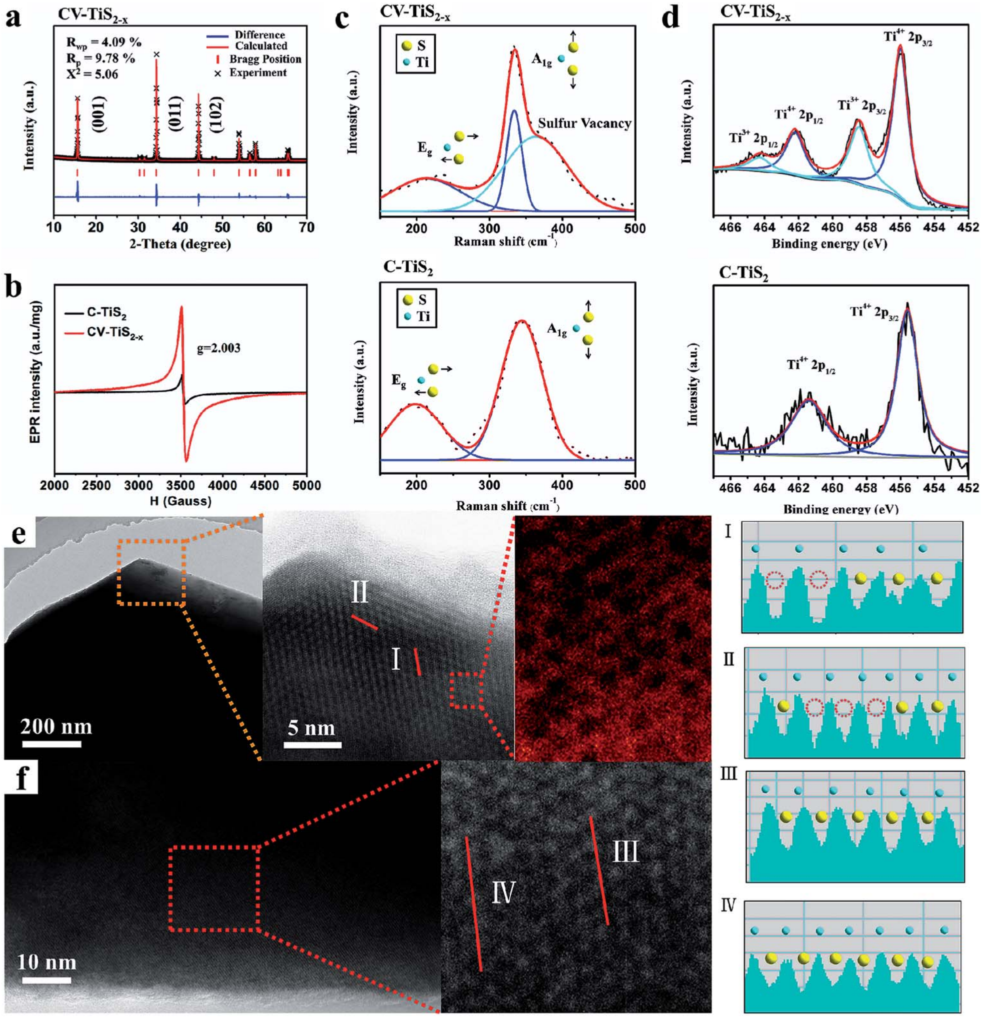

Fig. 2 XRD pattern of CV–TiS_{2-x} (a); EPR spectrum (b), Raman spectrum (c) and XPS analysis (d) of CV–TiS_{2-x} and C–TiS_2; TEM morphology and high-resolution diagram of CV–TiS_{2-x} (e) and C–TiS_2 (f); the presence of a sulfur vacancy can be proved by contrast analysis.

band, which indicates higher stability of the CV–TiS_{2-x} host structure in the ether-based electrolyte.

After continuous lithium ion intercalation and deintercalation in the crystal structure, the stacking faults of CV–TiS_{2-x} can be observed in the HRTEM image in Fig. 3b and the simulation of the crystal lattice in Fig. 3c. Additionally, the CV–TiS_{2-x} electrode was also characterized by *in situ* XRD in the 50th cycle (Fig. 3d). The distinct peaks with much higher intensity at about 14.5° indicate an expansion of the interlayer spacing of CV–TiS_{2-x} after cycling. The results demonstrate that CV–TiS_{2-x} maintains the crystal structure, but the interlayer is broadened to facilitate dynamic lithium ion intercalation and deintercalation of the CV–TiS_{2-x} electrode. In contrast, the *ex situ* XRD patterns of C–TiS_2 are shown in Fig. S8,† and the crystal structure collapsed after 50 cycles. Meanwhile, the XRD pattern of the CV–TiS_{2-x} electrode after 100 cycles is also shown in Fig. S9a.† Moreover, the electrodes and separators disassembled from the cycled C–TiS_2/Li and CV–TiS_{2-x}/Li cells are compared in Fig. S9b.† CV–TiS_{2-x} with abundant sulfur clusters shows a stable crystal structure in the ether-based electrolyte, which is very different from the reported sulfide.[35] The extended interplanar spacing during cycling contributes to a promoted Li-storage capability[36] and the dissolution of sulfide active materials is also mitigated, which guarantees the long-term cycling performance of CV–TiS_{2-x}. The high lithium-storage reaction kinetics and good electrochemical reversibility of CV–TiS_{2-x} are explained in Fig. 3e.

XPS measurements were performed on C–TiS_2 and CV–TiS_{2-x} after ten cycles to investigate the electronic environment, as shown in Fig. 4a and b. In order to eliminate the oxidation impurities on the surface induced by the transfer process, the sample was etched to 30 nm in the direction from the surface toward the particle center. In the sulfur spectrum of the C–TiS_2 electrode, the major component is Ti–S with S $2p_{3/2}$ and $2p_{1/2}$ doublets at 160.7 and 162 eV, respectively, which is similar to the original sample. However, a new doublet appears at low binding energies, 160 and 161.2 eV in the cycled CV–TiS_{2-x} sample, which is ascribed as $[S–S]^{2-}$. As is well-known, the reversible transformation between $[S–S]^{2-}$ and S^{2-} can provide additional capacity for the sulfide electrode.[37,38] Furthermore,

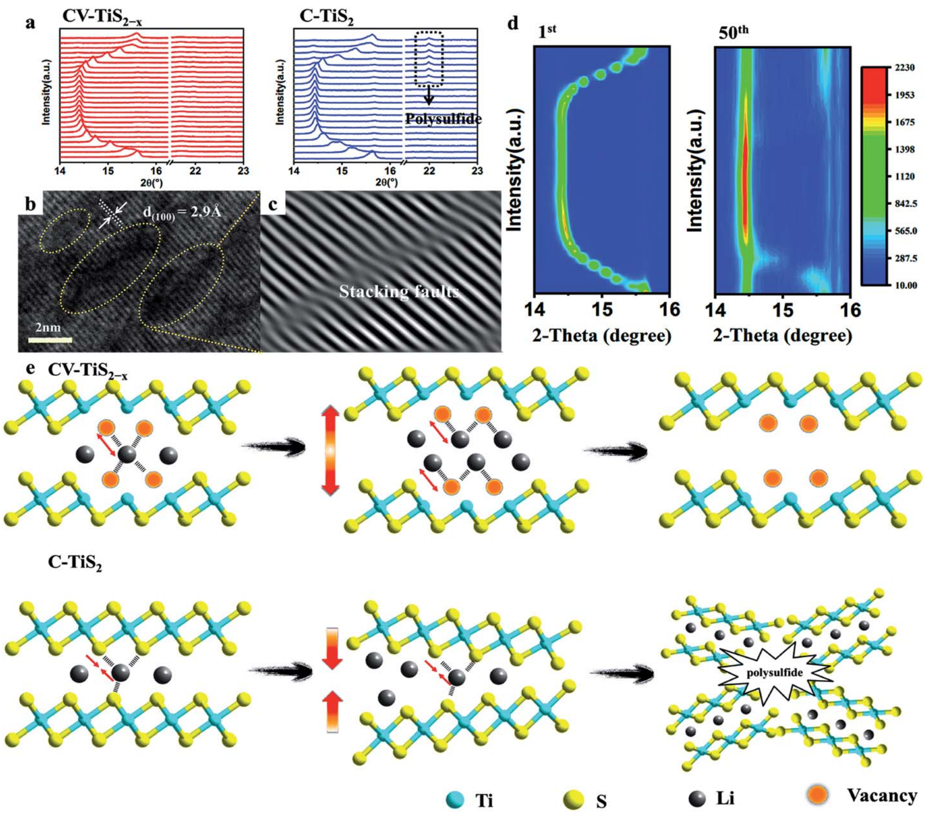

Fig. 3 Structural evolutions during lithiation and delithiation. *In situ* XRD patterns collected during the second discharge/charge processes of the Li/CV–TiS_{2-x} and Li/C–TiS_2 cell at the voltage range between 1.0 and 3.0 V (a). HRTEM image of the CV–TiS_{2-x} electrode after the 1st and 50th cycle (b) and the corresponding inverse fast Fourier transform (FFT) image (c). Structural evolution of CV–TiS_{2-x} during the initial and 50th lithiation/delithiation (d). The schematic illustration of the structural evolution of CV–TiS_{2-x} and conventional C–TiS_2 accompanied by the lithium–storage reaction (e).

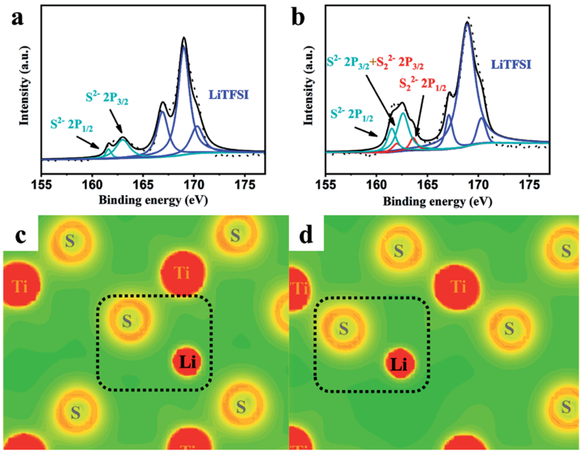

Fig. 4 XPS of C–TiS_2 and CV–TiS_{2-x}. Left: S 2p peak regions for C–TiS_2 (a). Right: S 2p peak regions for CV–TiS_{2-x} (b). Simulated charge-density distribution of C–TiS_2 and CV–TiS_{2-x} after lithium intercalation, where the red and green regions indicate charge accumulation and depletion, respectively (c and d).

the charge-density distributions of both the C–TiS_2 and CV–TiS_{2-x} sample after lithium intercalation were calculated by the DFT method (Fig. 4c and d). According to the Mulliken charge analysis, the charge dispersed on the Ti and S atoms is +1.474*e* and −0.822*e* for the C–TiS_2 sample, while the values change to +1.398*e* and −1.186*e* for the lithiated state, respectively. As a consequence, the Ti and S atoms theoretically capture 0.081 and 0.364*e* from each intercalated Li atom, respectively. Meanwhile, the charges on the Ti and S atoms are +1.494*e* and −0.851*e* for the cluster vacancy sample, but the Ti and S atoms get 0.077*e* and 0.471*e* from each intercalated Li atom. Compared with C–TiS_2, CV–TiS_{2-x} shows more electrons interacting with the sulfur atom, which indicates that the cluster vacancy contributes to enhancing the involvement of the anionic redox between $[S–S]^{2-}$ and S^{2-} during lithium intercalation.

The CV curves at the scan rate of 0.1 mV s^{-1} in Fig. 5a illustrate good coincidence of both the anodic and cathodic peaks, indicating a high electrochemical reversibility of CV–TiS_{2-x}. Detailed quantitative kinetics investigations of the C–TiS_2 and CV–TiS_{2-x} electrodes were also employed by the Galvanostatic Intermittent Titration Technique (GITT) and Electrochemical Impedance Spectroscopy (EIS) measurements. Fig. 5b and S10† show the GITT responses and the calculated apparent values of D_{Li^+} of CV–TiS_{2-x} and C–TiS_2, respectively. The CV–TiS_{2-x} sample exhibits a remarkably improved Li-ion diffusion coefficient (1.32×10^{-7} cm^2 s^{-1}), which is one order

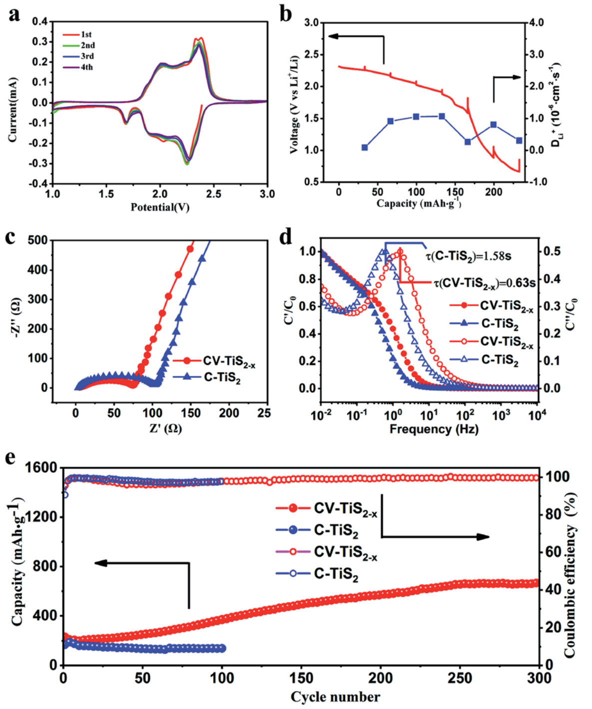

Fig. 5 The first four cyclic voltammetry curves for CV–TiS_{2-x} at a scan rate of 0.1 mV s^{-1} between 1.0 and 3.0 V (a). GITT curves of CV–TiS_{2-x} at the first cycle with a relaxation time of 2 h (b). Plot of the real and imaginary parts of the capacitance extracted from the Nyquist plots (c). The relaxation time of untreated C–TiS_2 and CV–TiS_{2-x} is 1.5 s and 0.6 s, respectively (d). Cycling performance of C–TiS_2 and CV–TiS_{2-x} (e).

of magnitude higher than those of C–TiS_2 and previous reports.[39] The Nyquist curves displayed in Fig. 5c show that CV–TiS_{2-x} exhibits a lower charge transfer resistance (12.6 Ω) than the C–TiS_2 sample (65.8 Ω) after cycling, confirming the superior electrochemical dynamics in the vacancy-rich CV–TiS_{2-x} electrode. What's more, the CV–TiS_{2-x} material exhibits the shorter relaxation time constant of $\tau(\text{CV–TiS}_{2-x}) = 0.63$ s in comparison with C–TiS_2 $\tau(\text{C–TiS}_2) = 1.58$ s, suggesting the much faster lithiation process in the CV–TiS_{2-x} electrode (Fig. 5d).

The cycling performances of CV–TiS_{2-x} and C–TiS_2 as electrodes for LIBs are also shown in Fig. 5e. CV–TiS_{2-x} delivers an initial discharge capacity of 220 mA h g^{-1} at 1C with a high initial coulombic efficiency of 91.3%. Subsequently, the electrode shows an increased capacity of 650 mA h g^{-1} after 300 cycles. In comparison, the C–TiS_2 displays a reversible capacity of less than 100 mA h g^{-1}, much more inferior cycling behavior than that of CV–TiS_{2-x}. Compared with other TiS_2 materials reported for lithium-ion batteries, CV–TiS_{2-x} also shows improved cycling performance and higher specific capacity (Table S3†). Fig. S11† exhibits the galvanostatic curves of the CV–TiS_{2-x} and C–TiS_2 samples during the first, and 50th cycles at a 1C rate. Moreover, the battery exhibits excellent capacity reversibility at the rate current of 25C, and the CV–TiS_{2-x} electrode can still deliver a high reversible capacity of 200 mA h g^{-1} (Fig. S12†).

TiS_2 with a sulfide cluster vacancy has been demonstrated herein to possess significantly improved reversibility in lithium storage processes. The enhanced Fermi level of CV–TiS_{2-x} can promote the chemical potential and stability of the TiS_2 host in the electrochemical system. Meanwhile, *in situ* XRD and HRTEM analysis indicate that the carrier transfer kinetics is boosted distinctly by the reduction of electrostatic interactions between Li^+ and sulfur anions in the host during the cycling process. The CV–TiS_{2-x} samples with plentiful positively charged S-vacancies exhibit an extended interplanar spacing during with cycling, leading to a high specific capacity. In addition, both Ti and S are involved in the redox reaction during the discharge and charge processes, which also facilitates lithium ion storage. Therefore, the CV–TiS_{2-x} materials show a gradually improved capacity and retain the structural integrity in continuous lithium ion intercalation and deintercalation. The CV–TiS_{2-x} with a stable host structure exhibits a high reversible capacity (650 mA h g^{-1}) after 300 cycles and a remarkable Li-ion diffusion coefficient (2.95×10^{-6} cm^2 s^{-1}) (Fig. S13†). Apparently, reversibly intercalating/deintercalating more than one lithium ion into a host lattice and simultaneously maintaining the crystal structure is realized in the TiS_2 phase with sulfide cluster vacancies.

Conclusion

Introducing abundant sulfur vacancies into TiS_2 leads to the reconfiguration of the electronic structure and a positive shift of the Fermi energy, which improves the electrochemical stability of CV–TiS_{2-x}. The stable crystal structure with a broadened interlayer space and enhanced anionic redox reaction activity during cycling ensured by the cluster vacancies facilitates the lithium intercalation and deintercalation in the host sulfide electrode and results in a significantly improved capacity. At a 1C current, CV–TiS_{2-x} delivers a high initial coulombic efficiency of 91.3% and a high capacity of 650 mA h g^{-1} after 300 cycles. TiS_2 with sulfide cluster vacancies is demonstrated as a promising electrode material for lithium metal batteries. Moreover, the application of vacancy chemistry can provide a new insight for boosting the capacity and simultaneously prolonging the life span of sulfide electrode materials.

Conflicts of interest

There are no conflicts to declare.

Acknowledgements

This work was financially supported by the National Natural Science Foundation of China (No. 51872026) and the Foundation of National Key Laboratory of Science and Technology on Power Sources (Grant No. 6142808020117C02).

Notes and references

1 T. Li, Y. H. Liu, B. Chitara and J. E. Goldberger, *J. Am. Chem. Soc.*, 2014, **136**, 2986–2989.

2 C. S. Cucinotta, K. Dolui, H. Pettersson, Q. M. Ramasse, E. Long, S. E. O'Brian, V. Nicolosi and S. Sanvito, *J. Phys. Chem. C*, 2015, **119**, 15707–15715.

3 E. A. Suslov, O. V. Bushkova, E. A. Sherstobitova, O. G. Reznitskikh and A. N. Titov, *Ionics*, 2016, **22**, 503–514.

4 E. Long, S. O'Brien, E. A. Lewis, E. Prestat, C. Downing, C. S. Cucinotta, S. Sanvito, S. J. Haigh and V. Nicolosi, *npj 2D Mater. Appl.*, 2017, **1**, 1–9.

5 M. S. Whittingham, *J. Solid State Chem.*, 1979, **29**, 303–310.

6 J. M. Tarascon and M. Armand, *Nature*, 2001, **414**, 359–367.

7 W. M. Stanley, *Chem. Rev.*, 2004, **35**, 4271–4301.

8 J. B. Goodenough and P. Kyu-Sung, *J. Am. Chem. Soc.*, 2013, **135**, 1167–1176.

9 L. Zhang, Q. Wei, D. Sun, N. Li, H. Ju, J. Feng, J. Zhu, L. Mai, E. J. Cairns and J. Guo, *Nano Energy*, 2018, **51**, 391–399.

10 M. S. Whittingham, C. Siu and J. Ding, *Acc. Chem. Res.*, 2018, **51**, 258–264.

11 Z. Hu, K. Zhang, Z. Zhu, Z. Tao and J. Chen, *J. Mater. Chem. A*, 2015, **3**, 12898–12904.

12 J. Lu, F. Lian, L. Guan, Y. Zhang and F. Ding, *J. Mater. Chem. A*, 2019, **7**, 991–997.

13 C. G. Hawkins and L. Whittaker-Brooks, *J. Mater. Chem. A*, 2018, **6**, 21949–21960.

14 B. Kiraly, N. Hauptmann, A. N. Rudenko, M. I. Katsnelson and A. A. Khajetoorians, *Nano Lett.*, 2017, **17**, 3607–3612.

15 H. S. Kim, J. B. Cook, H. Lin, J. S. Ko, S. H. Tolbert, V. Ozolins and B. Dunn, *Nat. Mater.*, 2017, **16**, 454–460.

16 T. Das, S. Chakraborty, R. Ahuja and G. P. Das, *ChemPhysChem*, 2019, **20**, 608–617.

17 W. Zhang, S. Shi, W. Zhu, C. Yang, S. Li, X. Liu, N. Hu, L. Huang, R. Wang, Y. Suo, Z. Li and J. Wang, *ACS Appl. Mater. Interfaces*, 2017, **9**, 32720–32726.

18 Y. Liu, T. Zhou, Y. Zheng, Z. He, C. Xiao, W. K. Pang, W. Tong, Y. Zou, B. Pan, Z. Guo and Y. Xie, *ACS Nano*, 2017, **11**, 8519–8526.

19 W. Xu, C. Sun, K. Zhao, X. Cheng, S. Rawal, Y. Xu and Y. Wang, *Energy Storage Materials*, 2019, **16**, 527–534.

20 J. Liu, H. Wang, C. Fang, L. Fu and X. Qian, *Nano Lett.*, 2017, **17**, 467–475.

21 Y. Guo, D. Liu and J. Robertson, *Appl. Phys. Lett.*, 2015, **106**, 173106.

22 D.-H. Seo, J. Lee, A. Urban, R. Malik, S. Kang and G. Ceder, *Nat. Chem.*, 2016, **8**, 692.

23 P. Peljo, J. A. Manzanares and H. H. Girault, *Langmuir*, 2016, **32**, 5765–5775.

24 M. Pandey, F. A. Rasmussen, K. Kuhar, T. Olsen, K. W. Jacobsen and K. S. Thygesen, *Nano Lett.*, 2016, **16**, 2234–2239.

25 Y. Zhang, Z. Mu, C. Yang, Z. Xu, S. Zhang, X. Zhang, Y. Li, J. Lai, Z. Sun, Y. Yang, Y. Chao, C. Li, X. Ge, W. Yang and S. Guo, *Adv. Funct. Mater.*, 2018, **28**, 1707578.

26 Y. Huang, K. Li, S. Li, Y. Lin, H. Liu and Y. Tong, *ChemistrySelect*, 2018, **3**, 7423–7428.

27 M. Inoue, H. P. Hughes and A. D. Yoffe, *Adv. Phys.*, 1989, **38**, 565–604.

28 A. Maiti and S. K. Srivastava, *J. Mater. Chem. A*, 2018, **6**, 19712–19726.

29 P. C. Sherrell, K. Sharda, C. Grotta, J. Ranalli, M. S. Sokolikova, F. M. Pesci, P. Palczynski, V. L. Bemmer and C. Mattevi, *ACS Omega*, 2018, **3**, 8655–8662.

30 K. Dolui and S. Sanvito, *EPL*, 2016, **115**, 47001.

31 Q. Ni, R. Dong, Y. Bai, Z. Wang, H. Ren, S. Sean, F. Wu, H. Xu and C. Wu, *Energy Storage Materials*, 2020, **25**, 903–911.

32 H. E. Wang, K. Yin, N. Qin, X. Zhao, F. J. Xia, Z. Y. Hu, G. Guo, G. Cao and W. Zhang, *J. Mater. Chem. A*, 2019, **7**, 10346–10353.

33 S. N. Li, J. B. Liu and B. X. Liu, *J. Power Sources*, 2016, **320**, 322–331.

34 H. Kim, K. Lim, G. Yoon, J.-H. Park, K. Ku, H.-D. Lim, Y.-E. Sung and K. Kang, *Adv. Energy Mater.*, 2017, **7**, 1700418.

35 H. Tao, M. Zhou, R. Wang, K. Wang, S. Cheng and K. Jiang, *Adv. Sci.*, 2018, 1801021.

36 H. Hwang, H. Kim and J. Cho, *Nano Lett.*, 2011, **11**, 4826–4830.

37 L. Zhang, D. Sun, J. Kang, H. T. Wang, S. H. Hsieh, W. F. Pong, H. A. Bechtel, J. Feng, L. W. Wang, E. J. Cairns and J. Guo, *Nano Lett.*, 2018, **18**, 4506–4515.

38 A. Grimaud, W. T. Hong, Y. Shao-Horn and J. M. Tarascon, *Nat. Mater.*, 2016, **15**, 121–126.

39 J. E. Trevey, C. R. Stoldt and S.-H. Lee, *J. Electrochem. Soc.*, 2011, **158**, A1282.